

# Dalton Transactions

Accepted Manuscript



This is an *Accepted Manuscript*, which has been through the Royal Society of Chemistry peer review process and has been accepted for publication.

*Accepted Manuscripts* are published online shortly after acceptance, before technical editing, formatting and proof reading. Using this free service, authors can make their results available to the community, in citable form, before we publish the edited article. We will replace this *Accepted Manuscript* with the edited and formatted *Advance Article* as soon as it is available.

You can find more information about *Accepted Manuscripts* in the [Information for Authors](#).

Please note that technical editing may introduce minor changes to the text and/or graphics, which may alter content. The journal's standard [Terms & Conditions](#) and the [Ethical guidelines](#) still apply. In no event shall the Royal Society of Chemistry be held responsible for any errors or omissions in this *Accepted Manuscript* or any consequences arising from the use of any information it contains.

# Encapsulation of Ni Salen Complex in Zeolite Y: An Experimental and DFT Study

*Archana Choudhary<sup>a</sup>, Bidisa Das<sup>b</sup> and Saumi Ray<sup>a\*</sup>*

<sup>a</sup> Birla Institute of Technology and Science, Pilani, Rajasthan 333031.

<sup>b</sup> Indian Association for the Cultivation of Science, Jadavpur, Kolkata 700032.

**Abstract:** It is observed that square planar Ni(II)–Schiff base complex of general formula {Ni(II)L}, where L is {L: *N,N'*-bis(5-hydroxy-salicylidene)ethylenediamine} when encapsulated in a supercage of zeolite Y, the bulky guest complex adopts a non-planar geometry without disturbing the integrity of the zeolite framework. Detailed comparative characterization is carried out to understand the structural change of the guest complex as a result of steric and electronic interaction with the host framework. UV-Vis spectroscopic studies of encapsulated and 'neat' complex shows significant blue shift in d-d transition after encapsulation and the diamagnetic 'neat' complex exhibits paramagnetism after encapsulation. DFT studies of Ni(II)–Schiff base complex have been carried out for different spin states in neat and encapsulated form and the UV-Vis spectra are simulated using TD-DFT to understand the observed spectra in details.

**KEYWORDS.** Zeolites, Encapsulation, Nickel(II) Schiff base Complex.

## Introduction

Zeolites are the micro porous aluminosilicate materials with cavities and channels of specific architectures, which have been extensively investigated for encapsulation of transition metal complexes, other organometallics, and polymers. Encapsulation provides a fascinating way of coupling the reactivity of the metal complex with the robustness and stereochemistry of the host zeolite framework,<sup>1-3</sup> which is nothing but an alternative route for the heterogenization of an otherwise homogeneous catalyst, with additional advantages like shape selectivity, site isolation, easy separation, resistivity at higher temperatures and better reactivity.<sup>4-8</sup> These hybrid catalysts have wide range of applications in gas purification, catalysis and biomimetic chemistry.<sup>9-11</sup> A fascinating subgroup of such encapsulated complexes are “ship-in-a-bottle” complexes, where building blocks of the complex are assembled together in the cavity of the porous solid and once synthesized, due to its size, the complex cannot 'leak out' through the pores without destruction of the framework.<sup>12</sup> It has already been well established that the space constraints imposed by the host framework can have profound influence on the structure of guest complex which can induce changes in magnetic, spectroscopic and redox properties of the encapsulated complex as compared to its properties in solution or in the solid-state leading to an enhanced reactivity or better selectivity from its solution state.<sup>13-17</sup> The catalytic activity of the encapsulated Schiff base complexes are well identified, they are potential heterogeneous catalyst for oxidation/epoxidation of alkanes, alkenes<sup>18</sup> and alcohols<sup>19</sup> with range of oxidants, *e.g.* tertbutylhydroperoxide (TBHP), hydrogen peroxide (H<sub>2</sub>O<sub>2</sub>), and molecular O<sub>2</sub>. P. Ratnasamy *et al* have reported that encapsulated copper salen and 5-chloro copper salen complexes in zeolite Y are efficient catalysts for oxidation of p-xylene, phenol and decomposition of TBHP and H<sub>2</sub>O<sub>2</sub>.<sup>20</sup> Recently, Deka *et al* have reported that encapsulated complex of Fe(III)-Schiff-base in zeolite Y

is efficient catalyst for oxidative coupling of 2-naphthol<sup>7</sup> and encapsulated complex of copper(II) salen in zeolite-Y shows enantioselectivity for Henry Reaction.<sup>21</sup> Phthalocyanine, porphyrine and salen complexes in zeolite Y are well known biomimetic systems and have the functional analogy with cytochrome P-450.<sup>9-11</sup> The encapsulation of FePc in zeolite-Y yields a catalyst which shows  $10^3$  times more activity for the oxidation of alkanes as compared to the its 'neat' form in solution.<sup>17</sup>

It is quite evident that the topology of the zeolite framework could have significant influence on the geometry of the guest molecule, which in turn could be correlated with the modified functionality of the system in terms of reactivity and selectivity. Relatively fewer reports are available in the literature exploring these aspects. Notably, Mizano *et al* have reported a novel temperature driven inter-conversion between a low-spin and a high-spin state of cobalt(II)tris(bipyridyl) complex encapsulated in zeolite Y.<sup>13</sup> Magnetic and spectroscopic studies of the  $[\text{Co}(\text{bpy})_3]^{2+}$  complex reveals that it adopts an octahedral geometry under encapsulation which is less distorted compared to its "free" state.<sup>22</sup> Mössbauer and optical spectroscopic studies of 6 coordinated  $\text{Fe}^{2+}$  complexes with a series of ligands have revealed that the complex of comparable size with that of the zeolite cavity undergoes trigonal prismatic distortion from octahedral geometry on encapsulation, whereas smaller complex doesn't show any such distortion.<sup>23</sup> A detailed study of Co phthalocyanine complex in "free" and encapsulated in zeolite-Y and MCM-41 had been carried out by Ray *et al*.<sup>24</sup> and it is observed that the encapsulated complex undergoes a saddle type distortion from planarity and the change in symmetry after encapsulation affects its magnetic behavior and shows enhanced magnetic moment than "neat" CoPc complex. Similar studies on  $[\text{Ni}^{\text{II}}\{\text{salnptn}(4\text{-OH})_2\}]$  complex, indicate

that the complex undergoes distortion under the influence of a constrained zeolite framework thus influencing the electronic structure of the molecular system.<sup>25</sup>

In the present study, we report the synthesis of encapsulated 5-OH-Ni(II) salen complex *via* flexible ligand synthesis method inside the zeolite Y and also in MCM-41 and detailed chemical, morphological and surface studies (XRD, SEM) along with spectroscopic (FTIR, UV-Vis) and magnetic studies of the encapsulated complex and the isolated complex are carried out. The observed shift in UV-Vis spectra as well as a drastic change in magnetic moment (diamagnetic when free and paramagnetic when encapsulated in zeolite) of the guest complex within the zeolite pore indicates that the geometry does not remain planar around the Ni centre. Theoretical studies of the geometry and electronic structure of 5-OH-Ni(II) salen complexes in different spin states are also carried out in free and encapsulated state using Density Functional Theory (DFT) for better understanding of the structure adopted by the complex and corresponding evaluation of the magnetic moment while entrapped within zeolite Y. Using TD-DFT methods we have simulated the UV-Vis spectra of the complex which helps in understanding the nature of the spectral transitions in the light of deformation of the square-planar guest complex upon encapsulation.

## Experimental Section

### Materials and Preparation

Zeolites Na-Y is purchased from sigma – aldrich, India. The chemicals used for synthesis Schiff base complex are 5 – hydroxy salicylaldehyde, ethylene di-amine (Alfa Aecer), nickel acetate and solvents (ethanol, acetone, methanol and diethyl ether) are purchased from S.D. fine, India. All chemicals and solvents are used as such without any further purification.

## Preparation of Schiff-Base Ligand

### Synthesis of *N,N'*-Bis(5-hydroxysalicylidene)ethylenediamine(5-OH-Salen)<sup>26</sup>

Two molar ratio of 5-hydroxy salicylaldehyde is dissolved in ethanol in 2 necks RB, and refluxed for 10 min, one molar ratio of ethylenediamine is added by syringe and refluxed again for 30 minutes at 60°C. A yellow crystalline solid product is obtained which is washed with ethanol and air dried. The purity of compound is analyzed by IR and UV – Vis spectroscopic techniques.

### Synthesis of Ni(II) Schiff base complex<sup>26</sup>(5-OH-NL5)

Equi molar mixture of 5-OH salen ligand in ethanol and nickel acetate dissolved in water (added to the ligand solution in drop-wise fashion) are mixed together and is refluxed. The reddish-brown product is then washed with ethanol and diethyl ether and finally dried at room temperature.

### Synthesis of Ni-exchanged zeolite Y.<sup>27-28</sup>

To prepare Ni-exchanged zeolite of desired loading level, measured quantity of zeolite-Y ( $\text{Na}_{58}\text{Al}_{58}\text{Si}_{136}\text{O}_{388}\cdot y\text{H}_2\text{O}$ ) is suspended in 0.01M nickel acetate solution and stirred at room temperature for 24 hours. The slurry is filtered, washed with hot distilled water until the filtrate is free from any metal ion adsorbed on the surface, and dried for 12 hours at 200 °C.

### Synthesis of encapsulated of Ni(II) Schiff-base complex in zeolite Y.<sup>7</sup>

Encapsulated Ni(II) complex is prepared by ‘flexible ligand’ method following the procedure reported in the literature<sup>7</sup> where the stoichiometric excess of ligand {*N,N'*-bis(5-hydroxy

salicylidene)ethylenediamine} is allowed to diffuse through the channels of Ni-exchanged zeolite and react to form the metal complex in the supercage. The mixture is refluxed for 24 hours at 180-200°C under constant stirring. The reddish brown solid mass is recovered and washed repeatedly with water, and dried at room temperature. To remove untreated species, impurities and surface species in zeolite framework, the dried mass is further purified by Soxhlet extraction using the solvents in sequence of acetone, methanol, and finally washing with diethyl ether until colourless solution is obtained in each case. The product is dried in a muffle furnace for 12 hours at 150°C.

### **Synthesis of MCM-41**

Synthesis of Al- MCM-41 is carried out according to the procedure<sup>29</sup> by keeping the molar ratio of sodium silicate and aluminum isopropoxide as 20: 1. Finally the suspension is transferred in polypropylene bottle and heated at 100°C for 4 days in furnace. After cooling to room temperature, material is recovered and repeatedly washed by deionized water, ethanol and calcinated overnight at 540°C.

### **Synthesis of encapsulated 5-OH-NL5 complex in MCM-41**

To synthesize 5-OH nickel salen complex encapsulated in MCM, the method discussed in section 2.2.4 is followed where the Ni(II) exchanged MCM-41 is refluxed with stoichiometric excess of ligand {*N,N'*-bis(5-hydroxy salicylidene)ethylenediamine} for 24 hours at 180-200°C with constant stirring. The reaction mass is further extracted by Soxhlet extraction by using acetone, methanol in sequence and then by diethyl ether and is finally dried in furnace at 150°C for 12 hours.

## Physical Measurements

Powder X-ray diffraction (XRD) patterns are recorded on a Shimadzu XD-D1 powder X-ray diffractometer using Cu K $\alpha$  radiation ( $\lambda = 1.542 \text{ \AA}$ ) for zeolite Y and Rigaku Ultima IV fully automatic high resolution X-ray diffractometer for MCM-41. XRD patterns are recorded in the  $2\theta$  range ( $8\text{--}50^\circ$ ) for zeolite Y and for MCM-41 ( $0\text{--}50^\circ$ ) at a scanning rate of  $2^\circ/\text{min}$ . The SEM – EDX analysis is carried out with Zeiss EVO 40 at an accelerated voltage of 5–20 kV, the samples are deposited on a brass holder and sputtered with gold. The electronic absorption spectra are recorded using a Shimadzu UV-2450 spectrophotometer with a diffuse reflectance accessory equipped with an integrating sphere of 60 mm inner diameter. To record the spectra of zeolite, “neat” and zeolite encapsulated metal complexes, the powdered samples are placed in a black absorbing spherical sample holder which has diameter of 10 mm. The UV-Vis spectra are recorded in the absorbance mode in the range of 190 nm to 700 nm using BaSO<sub>4</sub> as reference. The infrared spectra in the range  $450\text{--}4000 \text{ cm}^{-1}$  are recorded on ABB Bomen MB 3000 FTIR spectrometer. The spectra of the neat Ni-salen complex and the zeolite-encapsulated complex are recorded as KBr pellets. The magnetic studies have been done by using SQUID magnetometer Quantum Design MPMS XL EverCool, ZFC\_FC measurement in the temperature range of 5K to 300K.

## Theoretical Methods

All theoretical studies are performed using DFT as implemented in the GAUSSIAN 09, suite of *ab initio* quantum chemistry programs.<sup>30</sup> Geometry optimizations and vibrational frequency calculations are done using the hybrid B3LYP<sup>31-32</sup> exchange and correlation functionals and the double-zeta 6-31++G\*\* basis set for all atoms. Default SCF and geometry convergence criteria

are used and no symmetry constraints are imposed and all studies are performed at 298.1 K. Harmonic frequency analysis based on analytical second derivatives is used to characterize the stationary points on the potential energy surface. Theoretically we have modeled a portion Zeolite-Y supercage and all the dangling bonds of Si atoms are saturated using H atoms. The geometry of the zeolite supercage was kept fixed at the experimental structure but the hydrogen atoms were relaxed, such that a pre-optimized uncharged supercage was formed. Later for the studies involving, zeolite supercage and the encapsulated complex, we have allowed only the encapsulated complex to fully relax and attain the structure that is energetically lowest. The UV-Vis spectra of the complexes are calculated using time dependent density functional (TD-DFT) methods, considering both singlet and triplet spin states of the  $d^8$  Ni-complex. Transition energies and oscillator strengths for electronic excitation to the first 50 singlet or triplet excited states of the different complexes are calculated and analyzed for the free and encapsulated complexes and analyzed with the help of SWizard software<sup>33-34</sup>. For the triplet complex, the electrons with different spins behave differently and there are many transitions of which only triplet to triplet transitions are calculated. It is important to note that the Ni d-orbitals in the triplet case are strongly hybridized with the ligand pi orbitals and thus pure d-d transitions are hard to differentiate.

## Results and Discussions

### X-ray Powder Diffraction Studies

To ensure the preservation of zeolite framework integrity, as well as encapsulation of guest complex inside the cavity of the host, powder X-rays diffraction patterns of pure zeolite Y, (a); Ni-exchanged Y, (b); and encapsulated complex Ni(II) 5-hydroxy salen (c) are recorded (shown in Figure 1A). Essentially similar XRD patterns of these systems indicate the retention of integrity of zeolite framework during the encapsulation and even after the complex formation. A noticeable difference in the XRD patterns of zeolite Y with encapsulated complex from that of zeolite Y is an alternation in the relative intensities of peak positions of the 220 and 311 reflections ( $I_{220}$  and  $I_{311}$  respectively) appearing at  $2\theta = 10^\circ$  and  $12^\circ$ , respectively. For pure zeolite and Ni-exchanged zeolite the relation  $I_{220} > I_{311}$  holds, but for zeolite with encapsulated complex it is observed as  $I_{311} > I_{220}$ . This intensity reversal has already been identified and empirically correlated with the presence of a large complex within the zeolite-Y supercage.<sup>35-36</sup> The above study may suggest the presence of a large 5- OH-nickel salen complex inside the cavity of zeolite framework. No alternation of the peak intensities is observed for the complex formation occurring on the surface.<sup>23,37</sup> This change in the relative intensities may be associated with the rearrangement of randomly coordinated free cations in zeolite Y at different sites.<sup>25</sup> The above observations indicates successful encapsulation Ni(II) 5-hydroxy salen complex within void of the supercage Y. The XRD patterns of Al-MCM-41, Ni-Al-MCM-41 and encapsulated 5-OH-NL5 in MCM-41 are shown in Figure 1B. All three samples show very intense peak at  $2\theta = 0.68 - 0.70$ , that is indexed to 100 plane, the high intensity of 100 plane peak shows high degree of long-range order

and existence of uniform pores in the synthesized material.<sup>38-40</sup> Additional unresolved broader area is identified due to *110* and *200* planes. There is no further modification detected in nickel exchanged and encapsulated complex in MCM-41 XRD patterns, which clearly indicates the integrity of the MCM framework during the metal exchange and even encapsulation processes.

### Elemental Analysis

The unit cell formula of the parent sodium zeolite Y is  $\text{Na}_{58}\text{Al}_{58}\text{Si}_{136}\text{O}_{388}\cdot y\text{H}_2\text{O}$ . and Si/Al ratio is 2.34. EDX data indicate the unaffected Si/Al ratio even after exchange and encapsulation reactions. It signifies that the dealumination doesn't take place during encapsulation processes. The metal concentration in encapsulated complex is found to be lesser than ion exchanged zeolite Y, which directs towards the fact of participation of metal ions in coordination inside the cavities. Another possibility may be the leaching of some metal ions during the complex formation which causes the reduction metal-ion concentration. The general formula of Ni-exchanged zeolite-Y sample is  $\text{Ni}_x\text{Na}_{58-2x}\text{Al}_{58}\text{Si}_{136}\text{O}_{388}\cdot y\text{H}_2\text{O}$ . From AAS studies *x* is found to vary within 2 to 4. In the encapsulated complex the concentration of nickel metal is found less than 1 (0.68) wt percentage.

### Scanning Electron Microscopy

Encapsulation of nickel salen complex in zeolite Y is accomplished *via* flexible ligand synthesis method, to synthesize 'Zeozymes' where formation of the complex is essentially targeted inside the cavities of supercage not on the surface of the host framework. But formation of complex only inside the cavities is practically not viable, because some of the metal complexes can always be adsorbed on surface or some ligands may remain uncoordinated. To investigate surface morphology of zeolite Y specifically after encapsulation, SE micrographs of

encapsulated 5-OH-Ni-salen complex in zeolite Y before (Figure 2A) and after soxhlet extraction (Figure 2B) are analyzed and SEM images indicate, before extractions there are some visible surface species in the form of complexes or un-reacted ligands but are absent after extraction.<sup>7,25</sup> The particle boundaries on the external surface are clearly visible due to the complete removal of deposited adsorbed species on the surface in final product. The color of soxhlet extracted final product definitely is a sign of successful encapsulation of the complex inside the cavities of zeolite.

### Infrared Spectroscopy

The FTIR spectra of Na-zeolite-Y, encapsulated Ni(II) 5-hydroxy salen in zeolite-Y are shown in Figure 3A. IR spectrum of Na-zeolite-Y shows major bands in 450-1200  $\text{cm}^{-1}$  region with additional bands at 1643  $\text{cm}^{-1}$  and 3500  $\text{cm}^{-1}$  region. The major characteristics bands at 560, 717, 786, and 1018  $\text{cm}^{-1}$  are attributed to  $(\text{Si}/\text{Al}-\text{O})_4$  bending mode, double ring, symmetric stretching, asymmetric stretching vibration, respectively.<sup>7,41</sup> The broad bands observed at 3500  $\text{cm}^{-1}$  and 1643  $\text{cm}^{-1}$  are due to surface hydroxylic group and lattice water molecules respectively.<sup>25,42</sup> These bands are not significantly altered after the ion exchange and even after encapsulation of the complex inside the supercage, (indicated by asterisk in Figure 3A). This observation definitely suggests that the zeolite framework is remaining unaffected after encapsulation process. The characterization of encapsulated complex is somewhat difficult by IR spectroscopy because the intensity of IR bands of encapsulated complexes are very weak due to low concentration of complex inside the framework and zeolite bands interfere in proper observation of the complex. The region of 1200-1600  $\text{cm}^{-1}$  is appropriate to study because in this region, zeolite bands are almost silent and some of the prominent bands of the complex appear in this region with little shift in the peak positions. The expanded IR spectra (in range of 600-2000  $\text{cm}^{-1}$

<sup>1</sup>) are shown in Figure 3B and further expanded view (in the region of 1100-2000  $\text{cm}^{-1}$ ) is given in Figure 3C. The lower shift in the case of (C=N) and (C-O) stretching frequencies identify nitrogen and oxygen coordination inside the cavity of the zeolite framework.)<sup>43</sup> The  $\nu_{\text{C-H}}$  deformation bands at 1382  $\text{cm}^{-1}$  in case of encapsulated complex, are shifted towards higher wavenumbers, which indicate the encapsulation of the nickel Schiff-base complex inside the zeolite-Y.<sup>44</sup> The observed FTIR spectral data (Table 1) suggest the formation of a nickel Schiff-base complex in the 'free' as well as encapsulated state inside the supercage of zeolite.

### Theoretical Studies & Results

In the ground state the complex 5-OH-Ni(II) salen is planar<sup>45-47</sup> and exists as singlet with no unpaired electrons. The structure of the Ni-salen complexes in free state and then in encapsulated form are optimized and the resulting structures are shown in Figure 4. The geometrical parameters when compared with experimental XRD data show good agreement for the free complexes.<sup>48</sup> The isolated 5-OH-Ni(II) salen studied is planar and is more stable in singlet state without any unpaired electrons, but also can exist as a higher energy triplet state. The calculated energy difference between the triplet state and the singlet state for isolated 5-OH-Ni(II) salen is 21.47 kcal. After encapsulation, however, the non planer triplet state is substantially stabilized, but still remains less stable than the singlet state by 8.1 kcal. Due to the modest difference in energies, the possibility of a reasonable fraction of the complex existing in triplet state after encapsulation cannot probably be ruled out. Calculated spin density on Ni atom is 1.54 (total moment:  $2.35 \mu_{\text{B}} [n(n+2)]^{1/2}$ ) for the triplet 5-OH-Ni(II) salen. Apart from the ethylene linkage portion the singlet complexes are largely planar as appear in Figure 4. We report few selected bond lengths and bond angles obtained from geometry optimizations for the free and the encapsulated complexes in Table 2. It is seen that Ni-N distances vary from 1.87Å for the free

molecules and 1.84-1.85 Å for the encapsulated ones and Ni-O distances vary for 1.85-1.86 Å in free state whereas 1.84-1.85 Å when encapsulated. The O-C and N-C distances remain approximately 1.29 Å for both free and encapsulated cases. The bond angle O-Ni-N decreases from 94° to 93.2° in case of the singlet and 92.22° in case of the complex in triplet state. The angle C-Ni-C (marked in Figure 4 as rectangular boxes) is actually a measure of the planarity of the molecule in free or encapsulated state. This angle is 179.9° for the free singlet molecule, but decreases for the encapsulated one, with a large decrease to 165.3° in case of singlet and even larger decrease to 160.48° in case of the triplet state. The extent of bending is also clear from the end-to-end distances shown in Table 2, where the distance decreases from 14.3 Å to 13.7 Å (singlet) and 13.48 Å (triplet) when 5-OH-Ni salen is encapsulated in contrast to the free molecule. The change in the bond distances and bond angles on encapsulation may be attributed to the influence of the zeolite framework, where the topology of the supercage is expected to impose steric constraints on the complex.

The natures of the few important frontier molecular orbitals for the salen complexes as well as the optimized structures are presented in Figure S2 (ESI). In the free singlet molecule, the HOMO is mainly localized on  $p_z$  orbitals on N, O and C atoms along with  $d_{yz}$  on Ni which are responsible for a delocalized pi orbital. The LUMO mainly consists of p orbitals of O, N and C along with only a tiny contribution from Ni  $d_{xz}$  orbital.  $\text{HOMO}^{-1}$  and  $\text{LUMO}^{+1}$  orbitals are also primarily pi orbitals with only a small contribution from Ni  $d_{xz}$  for  $\text{HOMO}^{-1}$  and almost no Ni contributions for  $\text{LUMO}^{+1}$ .  $\text{HOMO}^{-2}$  is mostly localized on metal  $d_z^2$  while  $\text{LUMO}^{+2}$  is mostly localized on p and  $d_{xy}$  orbitals of Ni along with p orbitals of O and N.  $\text{HOMO}^{-3}$  is mainly p and  $d_{xz}$  on Ni and p on N, O and C atoms.  $\text{LUMO}^{+3}$  has no contributions from metal d orbital. The nature and the energies of the HOMO and LUMO for the free complex and those extracted from

zeolite are represented as a comparative energy diagram in Figure S3 (ESI). This figure also shows how the MO energies change after encapsulation for 5-OH-Ni salen singlet state and we find only a modest change in MO energies, in spite of bending. The molecular orbitals of the encapsulated triplet state of 5-OH-Ni(II) salen is shown in Figure S4, (ESI). In this case there are alpha and beta type of orbitals for up-spin and down-spin electrons, and it is seen from the Figure S4 that HOMO, HOMO<sup>-1</sup> and HOMO<sup>-2</sup> orbitals are contributed by Ni d orbitals and the C pi orbitals of salen. For the frontier unoccupied orbitals also Ni d contributes strongly along with C p orbitals *eg* LUMO, LUMO<sup>+1</sup> and LUMO<sup>+2</sup>.

The singlet state complex undergoes a considerable deviation from its planar geometry under encapsulation and the calculated gas phase TD-DFT spectrum of 5-OH-Ni salen complex both encapsulated (singlet) and encapsulated (triplet) are given in Figure 5a-b and the corresponding transitions are shown in Table 4. The nature of the spectra remains same for the isolated singlet and the encapsulated singlet cases but there are clear increase in transition energies and consequent decrease in wavelength of the first few transitions, namely isolated 5-OH-Ni salen: 652.8 nm (1.90 eV), encapsulated 5-OH-Ni salen 617.8 nm (2.01 eV); 559 nm (2.22 eV) and 532.6 nm (2.33 eV); 490.9 nm (2.53 eV) and 469.8 nm (2.64 eV) and few more with smaller shifts; all of which involves mainly the transition metal d orbitals. The first transition at 652.8 nm occurs primarily due to transition from HOMO to LUMO<sup>+2</sup> which is a d-d transition and the peak at 559 nm is due to transition from HOMO<sup>-2</sup> to LUMO<sup>+2</sup> which is again a d-d transition. A fairly intense HOMO to LUMO transition is observed at 478 nm also involved Ni d orbitals. It is these transitions which are mostly affected when the molecule is encapsulated, and the d-d transitions are observed at lower wavelengths for the encapsulated molecule and above transitions occur at 617.8, 532.2 and 469.8 nm respectively for the encapsulated case. When the

TDDFT spectrum of triplet 5-OH-Ni salen is considered we find that important d-d transitions occur at 594.6 (2.08 eV) and 540.6 nm (2.29 eV); of which the second one is reasonably intense in contrast to the isolated singlet case. Analysis of the spectral transitions and molecular orbitals (ESI, Figure S4) shows that the peak at 594.6 nm is due to transitions from HOMO to LUMO along with  $LUMO^{+1}$ ,  $HOMO^{-1}$  to LUMO and  $HOMO^{-2}$  to  $LUMO^{+2}$ . The intense peak at 540.6 nm is primarily due to transitions from HOMO to LUMO and  $LUMO^{+1}$ .

The experimentally obtained pore diameter of MCM-41 is  $\sim 68\text{\AA}$ , which is much larger compared to that of the zeolite supercage (pore size  $\sim 12.5\text{\AA}$ ). The end-to-end distance of the complex is  $\sim 14.3\text{\AA}$ . Thus even if the molecule aligns such that the full length is along the diameter of the pore, then the closest non bonded distances of the salen molecule and the wall of the pore is more than  $2.5\text{\AA}$ , thus only negligible confinement is offered by the pores. So it is expected that the singlet salen molecule would prevail in such a pore.

### UV-Visible Spectroscopy

For the better understanding of co-ordination environment and geometries of neat and encapsulated complexes, detailed UV-Vis spectroscopic studies are carried out in solution and solid state. For the solution UV-Vis study, chloroform has been selected as suitable solvent among others because it has been well established that Ni(II) salen complex shows distortion in solution with solvents of different dielectric constants like acetic acid, dichloromethane, methanol, chloroform etc. The minimum distortion is observed in chloroform.<sup>48</sup>

Comparative studies of electronic spectra of the 'neat' complex and that of the corresponding ligand reveal the presence of two additional bands at 361 and 437 nm of the complex,<sup>7</sup> which are assigned as charge transfer transitions. (experimental and DFT simulated UV-Vis data and

spectra of the ligand are given in ESI, Figure S5) The solid state (Figure 6A, Table 3) electronic transitions of the neat complex appearing at 240 nm is assigned as  $\pi-\pi^*$  transition and 332 nm as  $n-\pi^*$  transition. The strong evidence of free state complex formation is the appearance of charge transfer (CT) and d-d transitions bands, which are clearly observed in solid state electronic spectrum at 374, 424 and 590 nm respectively. Encapsulated Schiff base complex in zeolite shows  $\pi-\pi^*$  transition at 244 nm and  $n-\pi^*$  transitions at 288, 319, 337 nm. Charge transfer and d-d bands are appearing at 364, 384, 490 and 556 nm respectively. DFT simulated UV-Vis data supports above observations that these lower energy transitions which are assigned as CT and d-d bands have maximum contribution from metal center of the Schiff base complex. Some interesting observed features are associated with the d-d transition which is broader, more intense<sup>44</sup> and blue shifted in case of encapsulated complex with the comparison to that of the free state complex, which in turn provides evidence about the reshuffling in electronic energy levels probably because of the distorted geometry of the complex due to steric and electronic constraints imposed by host framework. Experimental spectrum of the encapsulated complex has a very similar nature of d-d transitions with that of the triplet state simulated spectrum where the bands are broader, more intense and blue shifted in comparison to that of diamagnetic neat singlet state encapsulated complex. (Figure 5a-b). This observation suggests that encapsulated guest complex has a different geometry around the metal center compared to that in its free state, and the geometry of guest complex is distorted and is probably present in paramagnetic triplet state.

A comparative UV-Vis study of encapsulated complex in MCM-41 and Zeolite Y has been done in solid state. The encapsulated 5-OH nickel salen complex in MCM-41 shows quite similar electronic behavior to that of the free state complex in chloroform rather than that of the complex

encapsulated in zeolite Y. (Figure 6B) The observation signifies the electronic environment of 5-OH-Ni(II) salen-MCM-41 is much closer to free state complex than encapsulated complex in zeolite Y. Although d-d bands are not very much clearly distinguishable of encapsulated complex in Al-MCM-41, but it is observed that the intensity of d-d region are not much increased and blue shifted as in case of encapsulated complex in zeolite Y. Such type intermediate electronic behavior from free and encapsulated state zeolite Y, of encapsulated complex in Al-MCM-41 can be explained in terms of less steric constrain imposed by the MCM-41 framework due to its large cavity (20 -100 Å) than zeolite Y (12.5Å).

### Magnetic Study

Both the electronic spectroscopic studies and theoretical studies indicate an alteration of the planar geometry of the guest complex when encapsulated in the zeolite-Y, mostly due to the space constraint induced by zeolite. On the other hand, the same studies on the complex encapsulated in the much larger pores of MCM-41, demonstrate significantly less distorted structure compared to that in zeolite. The unstrained neat Ni(II) salen and their derivatives are diamagnetic<sup>49-51</sup> with marginal distortion of the NiN<sub>2</sub>O<sub>2</sub> plane,<sup>49</sup> and expectedly the magnetic moments reported for these Ni(II) complexes turn out to be quite close to zero (ranging from 0.39 to 0.54  $\mu_B$ ), which essentially indicate presence of nearly planar NiN<sub>2</sub>O<sub>2</sub> moiety in them. To comprehend the effect of encapsulation particularly on the geometry around the metal ion, magnetic measurements are carried out. The  $\chi$  vs. T data have been fitted using the Curie-Weiss function along with a temperature independent paramagnetic component ( $\chi_0$ ) arising from Pauli and Van Vleck contributions. Figure 7 shows the temperature variation of inverse of the molar Curie-Weiss susceptibility ( $\chi-\chi_0$ ) for the 5-OH-Ni(II) Salen complex encapsulated in zeolite (black open circles) The linear behavior of the curve confirms paramagnetic behavior for this

complex, which must be arising solely from the metal complex, since the host is diamagnetic<sup>35,52</sup>. The moment calculated from the Curie constant for the zeolite encapsulated 5-OH-Ni(II) Salen comes out to be  $2.33 \mu_B$  and is very close to the moment obtained theoretically. From the theoretical studies a clear indication of lowering of the energy gap between the triplet and singlet states of the complex due to confinement of the complex inside zeolite is observed and the triplet state appears with the magnetic moment of  $2.35 \mu_B$  with the spin density on the Ni atom as 1.54. This large value of the moment from the Ni atom reveals that the encapsulation has indeed caused significant change in the  $\text{NiN}_2\text{O}_2$  plane (Figure 4) by shifting the Ni ion away from it and thereby making the higher lying excited triplet state much more accessible. As a result, considerable fraction of the complex molecules occupy the slightly higher lying excited triplet states (Section 3.5), which in turn gives rise to a higher moment of the complex. To have a better understanding about the origin of higher magnetic moment of the zeolite encapsulated complex, the magnetic studies of the complex encapsulated in larger pores of MCM-41 are also carried out. Curve (b) of Figure 7 shows the temperature variation of inverse Curie-Weiss molar susceptibility ( $\chi-\chi_0$ ) for the 5-OH-Ni(II) Salen complex encapsulated in MCM. However, the nonlinearity of this susceptibility curve indicates presence of other weaker magnetic contributions in this sample, visible only at higher temperature i.e. when the paramagnetic contribution is reduced. Fitting of the dominant low temperature paramagnetic contribution indicates a low magnetic moment of  $0.53 \mu_B$  in this sample. This value of the moment is exactly in agreement with the moment available in the literature<sup>46</sup> for such kind of systems in their neat forms, which essentially proves that the large pores of MCM are able to accommodate the complex without any further distortion. Therefore, the geometry adopted by the metal complex is expected to be the one observed in the free state.

## Conclusions

This manuscript presents a comparative spectroscopic and magnetic studies of the 5-OH-Ni(II) Salen complex encapsulated in hosts of different pore sizes like zeolite-Y, MCM-41 and in the un-encapsulated free state. The focus is on the effect of the size and topology of the pores of the host on the geometry adopted by the planar complex on encapsulation. Powder X-ray diffraction and vibrational spectroscopic studies support the successful encapsulation of the 5-OH-Ni(II) salen inside the supercage of zeolite-Y and in MCM-41 where the host frameworks remain intact. Electronic spectrum of the zeolite-Y encapsulated 5-OH-Ni(II) salen complex shows that charge transfer and *d-d* bands are mainly intensified and blue shifted whereas the spectrum of the complex in MCM-41 resembles quite closely to the solution spectrum taken in chloroform. The affected transitions which are closely associated with the metal center, indicates that the metal is shifted from the NiN<sub>2</sub>O<sub>2</sub> plane and the complex has adopted a distorted geometry which in turn, makes the energetically higher lying triplet state more accessible. Theoretical studies indeed show a significant stabilization of triplet state of the encapsulated complex compared to the free isolated singlet ground state. The theoretical magnetic moment calculated for the zeolite encapsulated complex in triplet state shows a magnetic moment of 2.35  $\mu_B$  with spin density on Ni as 1.54, whereas experimental magnetic moment is 2.33  $\mu_B$ . All these experimental and theoretical observations definitely prove that topology of the zeolite supercage has a pronounced effect on the structure of the complex. To fit into the cavity, the complex has undergone a distortion (as shown in Fig. 4c), as a result the energy gap between the triplet and singlet state is diminished, which causes a dramatic change of the magnetic property of the complex from diamagnetic to paramagnetic. This enhancement of the magnetic moment is clearly related to the extent of distortion of the 5-OH-Ni(II) salen from planarity, because the larger voids of

mesoporous MCM-41 encapsulates the complex without significant loss of planarity thereby leaving the complex diamagnetic as expected in its free state.

## Acknowledgements

The authors acknowledge the Department of Science and Technology, New Delhi, for the financial support (DST Project No: SR/FT/CS-038/2010) and for the instrumental facilities funded by DST-FIST, Department of Chemistry, BITS, Pilani and DST-FIST, Department of Physics, BITS, Pilani and for theoretical studies (DST Project No: SR/FT/CS-119/2010). The authors thank Prof. Sugata Ray for the helpful discussions

## Authors Information

<sup>a\*</sup>Dr. Saumi Ray, Assistant Professor, Department of Chemistry, Birla Institute of Technology and Science, Pilani Rajasthan -333031, INDIA. Fax: +91-(01596)244183; Tel:91-01596-515650; E-mail: [saumi@pilani.bits-pilani.ac.in](mailto:saumi@pilani.bits-pilani.ac.in).

<sup>a</sup>Archana Choudhary, Department of Chemistry, Birla Institute of Technology and Science, Pilani Rajasthan -333031, INDIA. Tel: 919462256701; E-mail: [archana.choudhary@pilani.bits-pilani.ac.in](mailto:archana.choudhary@pilani.bits-pilani.ac.in).

<sup>b</sup>Dr. Bidisa Das, Indian Association of Cultivation of Science, Jadavpur, Kolkata: 700032, India. Fax: 91 33 2473 2805; Tel:+91-033-24734971; E-mail: [cambd@iacs.res.in](mailto:cambd@iacs.res.in)

† Electronic Supplementary Information (ESI) available: [IR spectra of pure MCM-41 and encapsulated 5-OH-NL5 complex in MCM-41. The structure of the HOMO, LUMO molecular orbitals of 5-OH-NL5 complex. The molecular orbitals of complex in free and encapsulated

singlet state along with corresponding energy and the molecular orbitals of 5-OH-NL5 in encapsulated triplet state. The comparative experimental and TD-DFT simulated UV-Vis spectra of 5-OH salen ligand.]. See DOI: 10.1039/b000000x/

## References

- (1) (a) K. J. Jr. Balkus, A. G. Gabrielov, *J. Inclusion Phenom. Mol. Recognit. Chem.*, 1995, **21**, 159- 184; (b) P. K. Dutta, *J. Inclusion Phenom. Mol. Recognit. Chem.*, 1995, **21**, 215– 237; (c) C. R. Jacob, S. P. Varkey, P. Ratnasamy, *Appl. Catal. A*, 1999, **182**, 91– 96; (d) De D. E. Vos, P. P. Knops-Gerrits, R. F. Parton, B. M. Weckhuysen, P. A. Jacobs, R. A. Schoonheydt, *J. Inclusion Phenom. Mol. Recognit. Chem.*, 1995, **21**, 185– 213.
- (2) M. L. Cano, A. Corma, V. Fornés, H. García, M. A. Miranda, C. Baerlocher, C. Lengauer, *J. Am. Chem. Soc.*, 1996, **118**, 11006–11013.
- (3) M. Álvaro, J. F. Cabeza, A. Corma, H. García, E. Peris, *J. Am. Chem. Soc.*, 2007, **129**, 8074– 8075.
- (4) (a) N. Herron, *ChemTech.*, 1989, 542-548; (b) G. A. Ozin, C. Gil, *Chem. Rev.*, 1889, **89**, 1749-1764.
- (5) K. Kervinen, C. A. B. Pieter, M. B. Andrew, J. G. Gerbrand Mesu, G. Koten, J. M. K. G. Robertus, B. M. Weckhuysen, *J. Am. Chem. Soc.*, 2006, **128**, 3208– 3217.
- (6) C. K. Modi, P. M. Trivedi, S. K. Gupta, P. K. Jha, *J. Inclusion Phenom. Macrocyclic Chem.*, 2012, **74**, 117– 127.
- (7) K. K. Bania, D. Bharali, B. Viswanathan, R. C. Deka, *Inorg. Chem.*, 2012, **51**, 1657– 1674.
- (8) A. Corma, H. Garcia, *Eur. J. Inorg. Chem.*, 2004, 1143– 1164.

- (9) R. F. Parton, I. F. J. Vankelecom, M. J. A. Casselman, C. P. Bezoukhanova, J. B. Uytterhoeven, P. A. Jacobs, *Nature*, 1994, **370**, 541-543.
- (10) D. Srinivas, S. Sivasanker, *Catal. Surv. Asia*, 2003, **7**, 121– 132.
- (11) C. R. Jacob, S. P. Varkey, P. Ratnasamy, *Microporous Mesoporous Mater.*, 1998, **22**, 465– 474.
- (12) F. Bedioui, E. De Boysson, J. Devynch, K. J. Jr. Balkus, *J. Chem. Soc. Faraday. Trans.*, 1991, **87**, 3831-3834.
- (13) K. Mizuno, J. H. Lunsford, *Inorg. Chem.*, 1983, **22**, 3484– 3486.
- (14) K. K. Bania, R. C. Deka, *J. Phys. Chem. C*, 2011, **115**, 9601– 9607.
- (15) B. M. Weckhuysen, A. A. Verberckmoes, I. P. Vannijvel, J. A. Pelgrims, P. L. Buskens, P. A. Jacobs, R. A. Schoonheydt, *Angew. Chem. Int. Ed. Engl.*, 1995, **34**, 2652-2654.
- (16) R. Grommen, P. Manikandan, Y. Gao, T. Shane, J. J. Shane, R. A. Schoonheydt, B. M. Weckhuysen, D. Goldfarb, *J. Am. Chem. Soc.*, 2000, **122**, 11488-11496.
- (17) R. F. Parton, L. Uytterhoeven, P. A. Jacobs, *Stud. Surf. Sci. Catal.*, 1991, **59**, 395-403.
- (18) (a) M. J. Sabater, A. Corma, A. Domenech, V. Fornés, H. García, *Chem. Commun.*, 1997, **14**, 1285– 1286; (b) C. Jin, W. Fan, Y. Jia, B. Fan, J. Ma, R. Li, *J. Mol. Catal. A: Chem.*, 2006, **249**, 23– 30; (c) M. Silva, C. Freire, B. De Castro, J. L. Figueiredo, *J. Mol. Catal. A: Chem.*, 2006, **258**, 327– 333; (d) J. Poltowicz, K. Pamin, E. Tabor, J. Haber, A. Adamski, Z. Sojka, *Appl. Catal. A*, 2006, **299**, 235– 242.

- (19) (a) K.O. Xavier, J. Chackoa, K. K. M. Yusuff, *Applied Catalysis A*, 2004, **258**, 251–259;  
(b) M. R. Mauryaa, S. J. J. Titinchi, S. Chand, I.M. Mishra, *Journal of Molecular Catalysis A*, 2002, **180**, 201–209.
- (20) S. Deshpande, D. Srinivas, P. Ratnasamy, *Journal of Catalysis*, 1999, **188**, 261–269.
- (21) K.K. Bania, G.V. Karunakar, K. Goutham, R.C. Deka, *Inorg. Chem.*, 2013, **52**, 8017–8029.
- (22) S. K. Tiwary, S. Vasudevan, *Inorg Chem.*, 1998, **37**, 5239-5246.
- (23) Y. Umemura, Y.; Minai, T. J. Tominaga, *Phys. Chem. B*, 1999, **103**, 647-652.
- (24) S. Ray, S. Vasudevan, *Inorg Chem.*, 2003, **42**, 1711- 1719.
- (25) M. Jafarian, M. Rashvandavei M. Khakali, F. Gobal, S. Rayati, M. G. Mahjani, *J. Phys. Chem. C*, 2012, **116**, 18518– 18532.
- (26) S. D. Bella, I. Frágala, I. Ledoux, M. A. Díaz-García, T.J. Marks, *J. Am. Chem. Soc.*, 1997, **119**, 9550–9557.
- (27) K. Mori, K. Kagohara, H. Yamashita, *J. Phys. Chem. C.*, 2008, **112**, 2593-2600.
- (28) N. Herron, *Inorg Chem.*, 1986, **25**, 4714- 4717.
- (29) M. Selvaraj et al, *Journal of Molecular Catalysis A: Chem.*, 2002, **186**, 173-186.
- (30) M. J. Frisch et al, Gaussian 03, Revision C.02. Wallingford-CT 2004.
- (31) A. D. Becke, *J. Chem. Phys.*, 1993, **98**, 5648-5652.

- (32) A. D. Becke, *Phys. Rev. A*, 1998, **38**, 3098-3100.
- (33) S. I. Gorelsky, SWizard program, <http://www.sg-chem.net/>, University of Ottawa, Ottawa, Canada, 2013.
- (34) J. P. Holland, P. J. Barnard, S. R. Bayly, J. R. Dilworth, J. C. Green, *Inorganica Chimica Acta*, 2009, **362**, 402–406.
- (35) W. H. Quayle, J. H. Lunsford, *Inorg. Chem.*, 1982, **21**, 97– 103.
- (36) W. H. Quayle, G. Peeters, G. L. De Roy, E. F. Vansant, J. H. Lunsford, *Inorg. Chem.*, 1982, **21**, 2226– 2231.
- (37) K. K. Bania, R. C. Deka, *J. Phys. Chem. C*, 2012, **116**, 14295–14310.
- (38) X. S. Zhao, G. Q. Lu, G. J. Millar, *Ind. Eng. Chem. Res.*, 1996, **35**, 2075-2090.
- (39) R. Nares, J. Ramirez, A. Gutierrez-Alejandre, R. Cuevas, *Ind. Eng. Chem. Res.*, 2009, **48**, 1154-1162.
- (40) V. B. Fenelonov, et al, *J. Microporous and Mesoporous Materials*, 2001, **44-45**, 33-40.
- (41) B. Dutta, S. Jana, R. Bera, P. K. Saha, S. Koner, *Appl. Catal. A*, 2007, **318**, 89– 94.
- (42) R. M. Barrer, *Hydrothermal Chemistry of Zeolite*; Academic Press: New York, 1982.
- (43) M. Asadi, J.K. Aein, K.A. Hossein, *Inorganica Chimica Acta*, 2007, **360**, 1725-1730.
- (44) R. Ganesan, B. Viswanathan, *J. Phys. Chem. B*, 2004, **108**, 7102– 7114.

- (45) H. Yoon, T. R. Wagler, K. J. O'Connor, C. J. Burrows, *J. Am. Chem. Soc.*, 1990, **112**, 4568–4570.
- (46) J. E. Reed, A. A. Arnal, S. Neidle, R. Vilar, *J. Am. Chem. Soc.*, 2006, **128**, 5992–5993.
- (47) A. A. Arnal, J. Benet-Buchholz, S. Neidle, R. Vilar, *Inorg. Chem.*, 2008, **47**, 11910–11919.
- (48) M. A. Siegler, and M. Lutz, *Cryst. Growth Des.*, 2009, **9**, 1194–1200.
- (49) A. Böttcher, H. Elias, E. G. Jäger, H. Langfelderova, M. Mazur, L. Müller, H. Paulus, P. Pelikan, M. Rudolph, M. Valko, *Inorg. Chem.*, 1993, **32**, 4131–4138.
- (50) H. C. Zhang, W. S. Huang, L. Pu, *J. Org. Chem.*, 2001, **66**, 481–487.
- (51) H. Yoon, C. J. Burrows, *J. Am. Chem. Soc.*, 1988, **110**, 4087–4089.
- (52) D. N. Stamires, J. Turkevich, *J. Am. Chem. Soc.*, 1964, **86**, 749–757.

### Figure Captions

**Figure 1.** (A) Powder XRD pattern of (a) pure zeolite-Y, (b) Ni exchanged zeolite-Y, (c) Encapsulated 5-OH-NL5 in zeolite Y, (B) The XRD patterns of (a) Al-MCM-41, (b) Ni-Al-MCM-41 and (c) Encapsulated 5-OH-NL5 in MCM-41 at the range of  $(0 < 2\theta > 4)$ .

**Figure 2.** SE micrograph of encapsulated 5-OH-NL5 in zeolite Y, (A) before soxhelt extraction, (B) after soxhelt extraction.

**Figure 3.** (A) FTIR spectra in the range of  $500\text{ cm}^{-1}$  to  $4000\text{ cm}^{-1}$  of (a) pure zeolite Y, (b) encapsulated 5-OH-NL5 in zeolite Y (B) The FTIR spectra in the range of  $600\text{ cm}^{-1}$  to  $2000\text{ cm}^{-1}$  (a) pure zeolite Y, (b) encapsulated 5-OH-NL5 in zeolite Y, (c) “neat”5-OH-NL5 complex. (C) Enlarged view of FTIR spectra in the range of  $1100\text{ cm}^{-1}$  to  $2000\text{ cm}^{-1}$  (a) pure zeolite Y, (b) encapsulated 5-OH-NL5 in zeolite Y.

**Figure 4.** (a) 5-OH-NL5 molecule (singlet) free state (b) 5-OH-NL5 molecule (singlet) is encapsulated and extracted (c) 5-OH-NL5 molecule (triplet) is encapsulated and extracted. The atoms marked by the square defines the C-Ni-C bond angle. (d) The zeolite framework used for theoretical studies (e) 5-OH-NL5 molecule (triplet) is encapsulated within the zeolite pore. Closest non-bonding distance between 5-OH-NL5 and the zeolite framework is  $\sim 3.1\text{ \AA}$ .

**Figure 5.** Experimental and DFT simulated UV-Vis spectra of (a) DFT simulated singlet state (black vertical graph) and experimental encapsulated 5-OH-NL5 in zeolite Y, (red line graph) (b) DFT simulated triplet state (black vertical graph) and experimental encapsulated 5-OH-NL5 in zeolite Y, (red line graph).

**Figure 6.** (A) The solid state UV-Vis spectra of (a) 5-OH-NL5 (b) encapsulated 5-OH-NL5 in zeolite, (c) 5-OH-NL5 in chloroform (B) UV-Visible spectra of (a) “neat” 5-OH-NL5 in chloroform (b) encapsulated 5-OH-NL5 in complex in MCM-41.

**Figure 7.** The  $1/x-x_0$  Vs T graph of (a) 5-OH-NL5 complex in zeolite Y and (b) 5-OH-NL5 complex in MCM-41.

## Figures

Figure 1

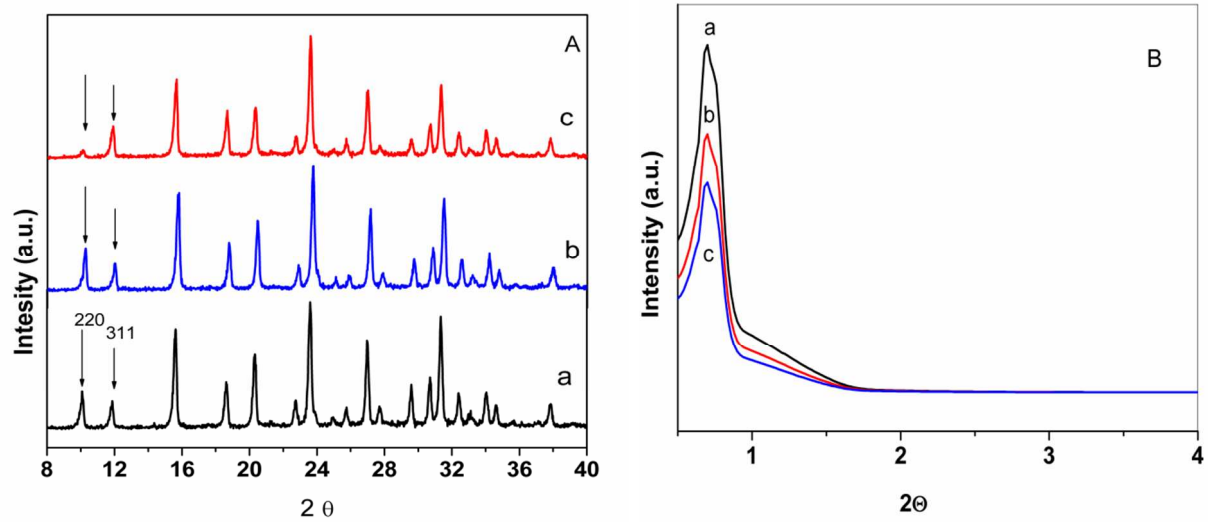


Figure 2

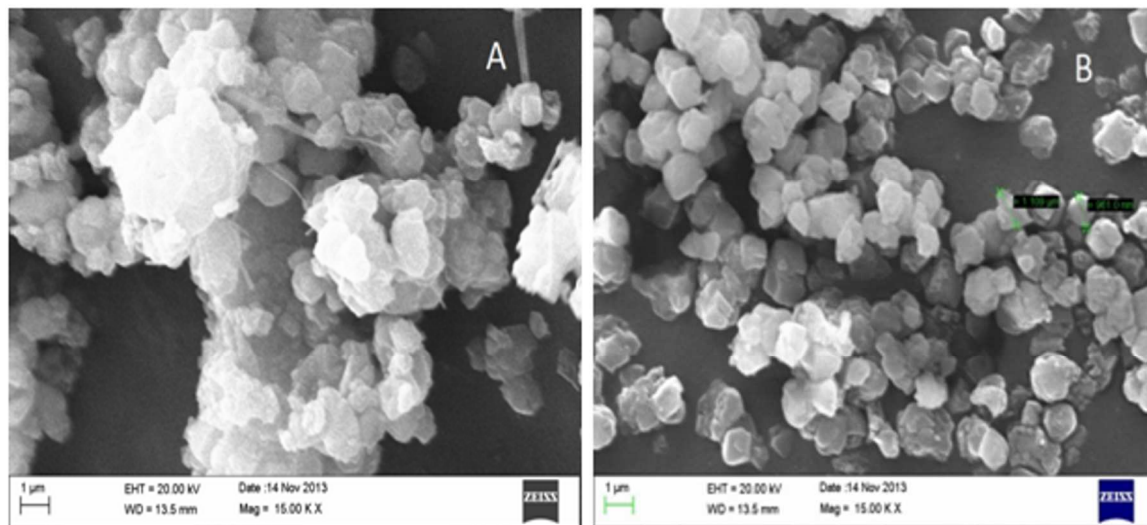


Figure 3

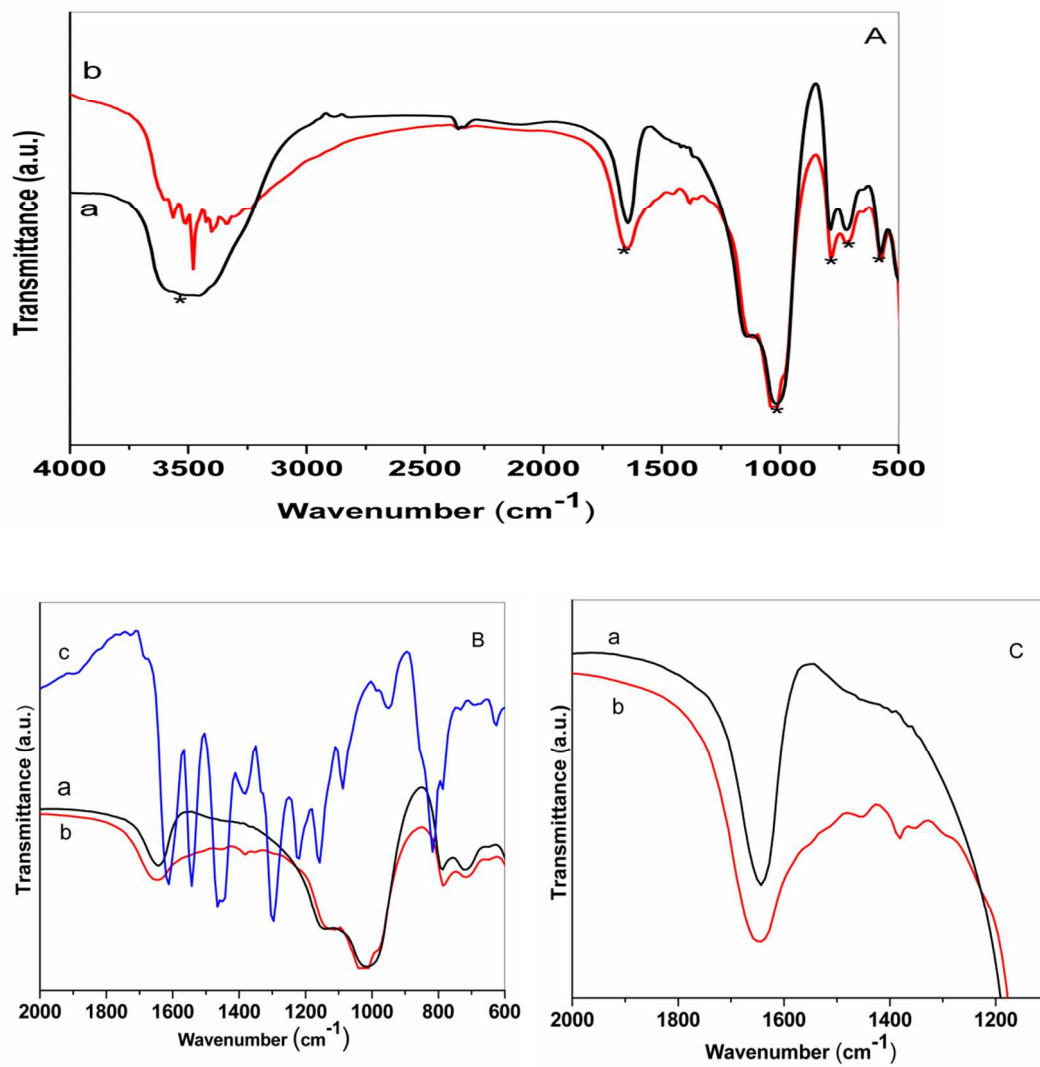


Figure 4

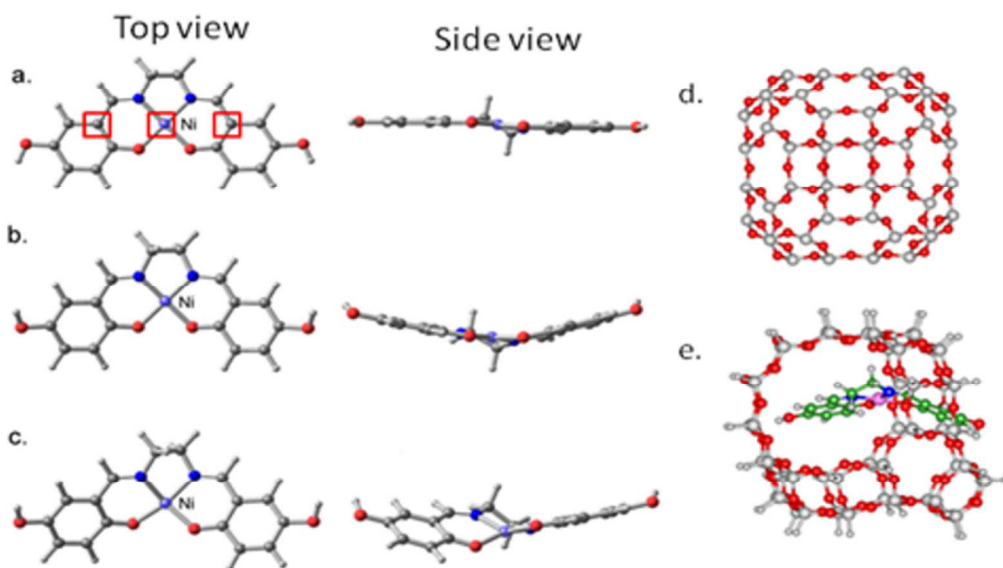


Figure 5

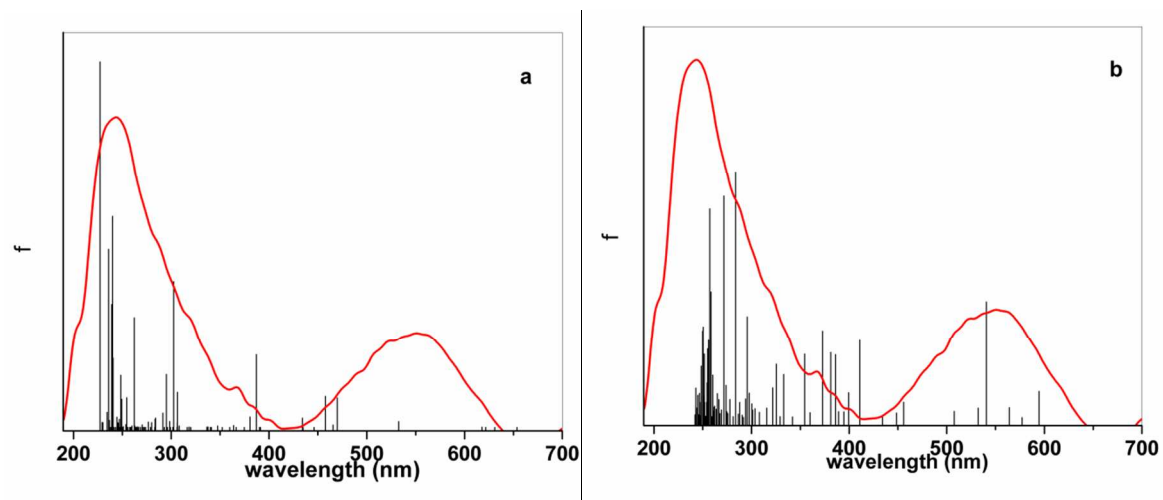


Figure 6

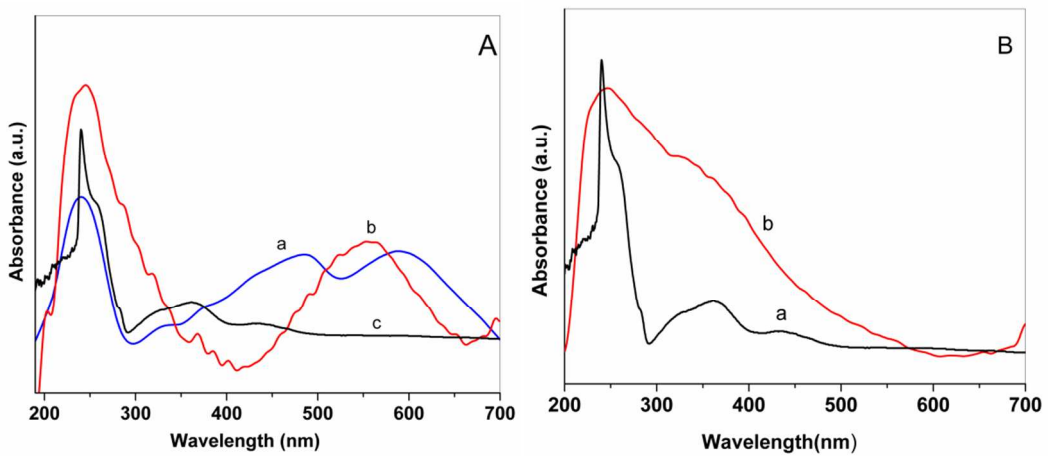
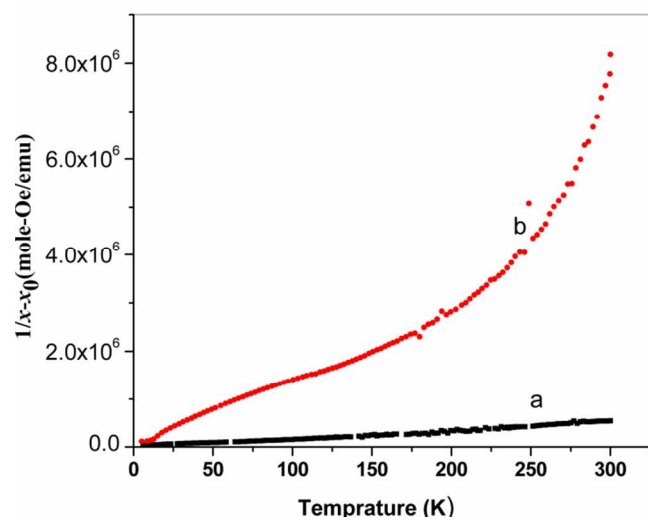


Figure 7



## TABLES

**Table 1.** FTIR spectral data (in  $\text{cm}^{-1}$ ) for the “neat” and encapsulated 5-OH- NL5- complex.

Sample	(C=N stretching)	(C=C stretching )	( $\nu_{\text{C-H}}$ deformation)	(C-O stretching)
5-OH-salen ligand	1635	1580,1481	1381	1352
“Neat” 5-OH-NL5	1620	1542, 1465	1375	1332
Encapsulated 5-OH-NL5 in zeolite Y	1642	1551, 1451	1382	1301

**Table 2.** Important geometrical parameters and molecular orbital's for 5-OH-NL5 in free and encapsulated case.

Bond distances(Å)/ angles( <sup>0</sup> ) /Energy (eV)	5-OH-NL5  free singlet	5-OH-NL5  encapsulated in zeolite  Singlet	5-OH-NL5  encapsulated in zeolite Triplet
Ni-O (Å)	1.85	1.83	1.88
Ni-N (Å)	1.87	1.85	1.97
O-C (Å)	1.30	1.30	1.30
N-C(conj) (Å)	1.30	1.30	1.30
<O-Ni-N	94.0	93.2	92.22
<C-Ni-C	179.9	165.3	160.48
End to end distance (Å)	14.32	13.70	13.48
HOMO (eV)	-4.97	-5.03	-5.32, -5.46
LUMO(eV)	-1.86	-1.88	-1.93, -2.35
HOMO-LUMO gap (eV)	3.11	3.14	3.39, 3.11

Table 3

**Table 3.** UV-Vis data of the “neat” and encapsulated 5-OH- NL5 in zeolite Y in solid state.

Complex	$\pi-\pi^*$ transitions	$n-\pi^*$ transitions	Charge transfer transitions	d-d transitions
“Neat” 5- OH-NL5	240	332, 376	424, 485,	590
Encapsulated 5-OH-NL5 in zeolite Y	244	288, 319, 337	364, 384, 490	556

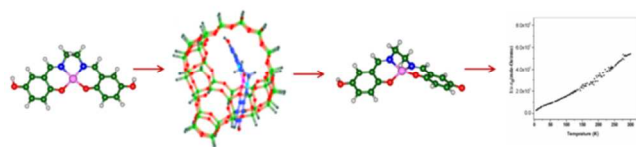
**Table 4.** UV-Vis experimental and TD-DFT simulated spectral data of the “neat” and encapsulated 5-OH-NL5 in solid state with corresponding assignments.

(5-OH-NL5) in chloroform	solid state (5-OH-NL5)	DFT (5-OH-NL5) singlet	Transitions (singlet)	(Encapsulated 5-OH-NL5 in zeolite Y) solid state	DFT (Encapsulated 5-OH-NL5 in zeolite Y) singlet	Transitions (singlet)	DFT(Encapsulated 5-OH-NL5 in zeolite Y) triplet	Transitions (triplet)
240 (258 sh)	240 (s)	295	$H^5-L^0$	244	295	$H^5-L^0$	257	$H^4-L^{+1}$ $H^0-L^{+5}$
		301	$H^3-L^{+1}$ $H^5-L^0$		302	$H^3-L^{+1}$ $H^5-L^0$ $H^4-L^0$	271	$H^4-L^0$ $H^3-L^0$
328	332	351	$H^0-L^{+2}$ $H^2-L^0$ $H^4-L^{+2}$	288	336	$H^0-L^{+2}$ $H^2-L^0$ $H^4-L^{+2}$	283  295	$H^4-L^{+2}$ $H^6-L^{+2}$ $H^3-L^{+2}$  $H^1-L^{+2}$ $H^5-L^{+1}$ $H^3-L^{+1}$
361		365	$H^2-L^0$ $H^0-L^{+2}$ $H^4-L^{+2}$		363	$H^2-L^{+0}$	325  322	$H^7-L^0$ $H^0-L^{+5}$  $H^3-L^0$ $H^2-L^0$ $H^4-L^0$
	376	387	$H^1-L^{+1}$	319, 337	380	$H^1-L^{+1}$	354	$H^0-L^{+3}$ $H^1-L^{+3}$
							373	$H^2-L^0$ $H^1-L^{+2}$ $H^0-L^0$
		395 446	$H^1-L^0$  $H^5-L^{+1}$ $H^{11}-L^{+2}$	364 384	387 434	$H^1-L^{+0}$  $H^5-L^{+2}$ $H^{11}-L^{+2}$ $H^9-L^{+2}$	386  381	$H^1-L^{+2}$ $H^0-L^{+2}$ $H^1-L^{+1}$ $H^0-L^{+1}$  $H^0-L^{+2}$ $H^1-L^{+2}$
437	424	465	$H^0-L^{+1}$		457	$H^0-L^{+1}$ $H^0-L^{+2}$	411	$H^1-L^{+1}$ $H^1-L^{+0}$ $H^0-L^{+1}$
	485	478	$H^0-L^0$ $H^2-L^{+2}$	490	469	$H^0-L^0$ $H^2-L^{+2}$	456	$H^0-L^0$ $H^0-L^{+1}$
		490 559	$H^3-L^{+2}$ $H^7-L^{+2}$ $H^1-L^{+2}$  $H^2-L^{+2}$ $H^0-L^0$		465 532	$H^3-L^{+2}$ $H^7-L^{+2}$ $H^1-L^{+2}$ $H^0-L^{+1}$  $H^2-L^{+2}$ $H^0-L^0$	540  594	$H^0-L^0$ $H^0-L^{+1}$ $H^0-L^0$ $H^0-L^{+1}$ $H^1-L^0$ $H^2-L^{+2}$



## Table of contents

## Encapsulation of Ni Salen Complex in Zeolite Y: An Experimental and DFT Study

*Archana Choudhary<sup>a</sup>, Bidisa Das<sup>b</sup> and Saumi Ray<sup>a\*</sup>*\*Corresponding author email id.: [saumi@pilani.bits-pilani.ac.in](mailto:saumi@pilani.bits-pilani.ac.in)

Planar diamagnetic Ni-complex when encapsulated in zeolite Y adopts nonplanar geometry and shows pragmatic change in its magnetic property.